Research article

Morphology of the collapse scar of the Chiles Volcano (Colombia-Ecuador border) and geomechanical characterization of rock masses

Morfología de la cicatriz de colapso del Volcán Chiles (Frontera Colombia-Ecuador) y caracterización geomecánica de macizos rocosos

Laura Viviana **Paez**[1]✉, John J. **Sánchez**[2]✉, Álvaro Jesús **Castro-Caicedo**[3]✉

[1]Departamento de Geociencias, Universidad Nacional de Colombia-Sede Bogotá, Bogotá, Colombia
[2]Departamento de Geociencias y Medio Ambiente, Facultad de Minas, Universidad Nacional de Colombia-Sede Medellín. Medellín, Colombia
[3]Departamento de Materiales y Minerales, Universidad Nacional de Colombia-Sede Medellín, Medellín, Colombia

ABSTRACT

Chiles Volcano is an active stratovolcano of the Cordillera Occidental in a dormant state built by accumulation of andesitic-dacitic lava flows, which was affected by a large lateral collapse on its northern flank that subsequently generated one or multiple volcanic debris avalanches (VDAs). As a result of the morphological analysis of the collapse scar, it is proposed that this lateral collapse may have been caused by factors unrelated to the volcano's eruptive activity, which impacted the stability of the volcanic structure. This geomorphological study marks a significant step forward in understanding lateral collapses in an area where sedimentological data about the VDAs is extremely limited due not only to the complexity of the topography, but also to the glacial and fluvial processes of the area. The descriptive and geometric analysis of the scar resulting from the collapse indicates that this morphological expression is U-shaped and deep-seated and has the following dimensions: length = 3.0 km, width = 1.6 km, height = 0.8 km, and aperture angle = 31°. Respectively, the area and volume of material involved in the collapse are estimated at 4.0 km² and 0.5 km³. The geomechanical characterization of the Chiles Volcano rocks was done in five outcrops located on the southern flank applying either the Rock Mass Rating (RMR) or the Geological Strength Index (GSI); additionally, these values obtained in the field were complemented with results from other studies in the area, which encompass the eastern and northern flanks of the volcano. GSI values for columnar, brecciated, and blocky lava flows range between 47–72; 15–65 and 37–57, respectively. Using triaxial tests by the multiple failure state method, the compressive strength of the rock mass was 24.92 MPa; respectively, cohesion and internal friction angle values were 4.21 MPa and 51.95° for peak strength, and 1.52 MPa and 52.4° for residual strength.
Keywords: Collapse scar, rock quality, volcanic edifice, debris avalanche, flank stability, volcanic hazard.

RESUMEN

El Volcán Chiles es un estratovolcán activo de la Cordillera Occidental en estado de reposo constituido a partir de la acumulación de flujos de lava andesítico-dacíticos, el cual fue afectado por un gran colapso lateral en su flanco norte que posteriormente generó una o múltiples avalanchas de detritos volcánicos. Como resultado del análisis morfológico de la cicatriz del colapso, se propone que este colapso lateral pudo haber sido causado por factores ajenos a la actividad eruptiva del volcán que impactaron la estabilidad de la estructura volcánica. Este estudio geomorfológico marca un importante aporte en la comprensión de los colapsos laterales en una zona donde los datos sedimentológicos de las avalanchas de detritos volcánicos son extremadamente limitados debido no sólo a la complejidad de la topografía, sino también a los procesos glaciares y fluviales de la zona. El análisis descriptivo y geométrico de la cicatriz producto del colapso indica que esta expresión morfológica tiene forma de U y es profundamente arraigada; tiene las siguientes dimensiones: largo = 3.0 km, ancho = 1.6 km, altura = 0.8 km y ángulo de apertura = 31°. El área y volumen de afectación de edificio volcánico por el colapso se estiman respectivamente, en 4.0 km² y 0.5 km³.

La caracterización geomecánica de las rocas que constituyen el Volcán Chiles se realizó en cinco afloramientos localizados en el flanco sur aplicando, según el caso, el Sistema de Clasificación del Macizo Rocoso (Rock Mass Rating – RMR) o el Índice de Resistencia Geológica (Geological Strength Index – GSI); adicionalmente, estos valores obtenidos en campo, se complementaron con los resultados de otros estudios geomecánicos realizados en el área, los cuales abarcan los flancos este y norte del volcán. Los valores de GSI para flujos de lava con disyunción columnar, brechificados y en bloques están en los rangos 47 – 72; 15 – 65 y 37 – 57, respetivamente. Como resultado de las pruebas de compresión triaxial por método de falla múltiple, se obtuvo que la resistencia a la compresión del macizo rocoso es de 24.92 MPa, con valores de cohesión y de ángulo de fricción interna, respetivamente, de 4.21 MPa y 51.95° para la resistencia pico y, 1.52 MPa y 52.4° para la resistencia residual.
Palabras clave: Cicatriz de colapso, calidad de la roca, edificio volcánico, avalancha de detritos, estabilidad del flanco, amenaza volcánica.

1. INTRODUCTION

Lateral collapses to which structures of volcanic origin are susceptible have been recognized globally for around 600 volcanoes in different geological environments, mostly of Quaternary age, with 1001 cases identified in the most recent inventory (Siebert and Roverato, 2021). It is proposed that the single or multiple fault surfaces on which the movement of the material occurs as a result of the lateral collapse can reach hundreds of meters deep in a volcanic edifice, removing volumes from 0.2 to 4.2 km^3 and generating deposits that cover areas between 8 and 176 km^2, as per the cases studied in various volcanic areas around the world (this for VDAs that occurred since 1500 AC) (Siebert and Roverato, 2021).

In Colombia, volcanic debris avalanche (VDA) deposits have been reported at Nevado del Ruiz, Nevado del Tolima, Cerro Machín, Nevado del Huila, Sotará, Galeras, Azufral, Cumbal, and Chiles-Cerro Negro volcanic complexes (Joya, 2013; Moreno et al., 2020; Monsalve-Bustamante, 2020).

The focus of the present work was the Chiles Volcano (Figure 1), which was built mainly by the accumulation of andesitic-dacitic lava flows. It was affected by a large lateral collapse on the northern flank, which generated a single or multiple subsequent VDAs. Velásquez and Parra (2002) suggest that this collapse occurred over 20,000 to 25,000 years ago, as evidenced by a glacial event reaching 3200 meters above sea level (m.a.s.l.) in the area. This event corresponds to the Murillo Glacier Stage (Van der Hammen, 1981, as cited in Velásquez and Parra, 2002), which extended to 3400 m.a.s.l. in the Central Cordillera (Colombia) and is associated with the Last Glacial Maximum (LGM).

A future collapse in the Chiles Volcano could have serious consequences. The current hazard zoning for VDAs in the Chiles Volcano includes urban, rural, and tourist areas near the volcano (Servicio Geológico Colombiano (SGC), 2014). According to the above, the interdisciplinary study of these events is crucial for assessing geological risks and constructing collapse simulation models due to their potential large-scale effects. This importance is underscored by extensively documented instances like that of Mount Taranaki in New Zealand, a volcano situated within Egmont National Park, drawing a significant number of tourists. While classified as dormant and possessing a stable structure, it still holds latent hazards regarding VDAs (Procter et al., 2010; Procter et al., 2021; Mead et al., 2022).

The study of the deposits and their origin areas, in addition to the morphological characterization of the structures related to a lateral collapse (hummocks, toreva blocks and collapse scar; Bernard et al., 2021), allows the identification and analysis of this

process. The term "hummocks" describes a group of hills with diverse shapes and sizes, forming a distinctive surface feature of VDA deposits. When these hummocks are elongated, they're termed as ridges. If the hummock primarily consists of intact pieces of removed material, typically longer than 1 kilometer, and has undergone minimal movement with a slight rotation, they're referred to as toreva blocks (Bernard et al., 2021).

Collapse scars are distinctive morphological features that typically exhibit a wide opening angle and, in some instances, parallel or non-parallel lateral walls that cover the top of the volcano edifice (Bernard et al., 2021). This attribute can be the only source of information about a lateral collapse where the VDA deposits have been eroded, as is the case of the deposit produced by the collapse of the northern flank of Chiles Volcano.

In complex geological settings, like those shaped by tectonic movements and erosion, collapse scars examples are founded where volcanic landscapes have undergone complete transformation. Here, features like collapse scars stand out due to their size, shape, and remarkable preservation over time. For instance, the Miocene collapse scar observed in the Keserus Hill volcano in Hungary (Karátson et al., 2006) serves as a crucial element in comprehending present-day geomorphology.

Similarly, in regions like the Călimani-Gurghiu-Harghita volcanic range in Eastern Transylvania, Romania (Seghedi et al., 2023), collapse scars play a key role not only in understanding current landscape formations but also in characterizing volcaniclastic deposits like VDA deposits.

In this work, the collapse scar of the volcano, which was preliminarily delineated in previous works (Perdomo et al., 1986; Parra and Velásquez, 2003), is described, delimited with greater accuracy, and geometrically characterized based on the methodology of Bernard et al. (2021).

Regarding the origin of lateral collapses, a current topic debate in the volcanological community, these can or cannot be associated with volcanic activity (Bernard et al., 2021). Different processes contribute to the destabilization of a volcanic edifice: the action of different types of stress, the gravitational load exerted by the material of the edifice, the dynamic loads due to seismic activity, the alteration of the rocks by hydrothermal circulation, regional stress fields, among other factors.

Additionally, there is evidence that lateral collapses can occur during periods of volcanic inactivity or even when the volcano is extinct (van Wyk de Vries and Davies, 2015). In the most recent inventory of these events, around a fifth of the currently recorded lateral collapses occurred without eruptive activity (Siebert and Roverato, 2021).

Chiles Volcano locates within a tectonically active zone, with evident alteration of rock masses, showing intense localized

hydrothermal activity, and an increase in seismic activity since 2013 (Servicio Geológico Colombiano (SGC), 2021); in addition, it has been affected by processes of intense weathering and erosion because of the harsh weather conditions and the lack of vegetation cover its upper flanks. The Chiles Volcano area is classified as extremely cold humid (Caldas-Lang Climate Classification; Instituto de Hidrología, Meteorología y Estudios Ambientales (IDEAM), n.d.-a).

According to the records of the Chiles rainfall station (Cumbal, Nariño), located at 3100 m.a.s.l., for the period 1991-2020, precipitation in the area presented an annual average of 1103.4 mm, with a total of 147.2 days of rain annually (IDEAM, n.d.-b). Considering this, the research into external factors affecting the stability of volcanic structures assumes significance due to rainfall and the resulting fluvial and hydrogeological activity in the region. Understanding these external influences is crucial in comprehending lateral collapses.

Recently, different methods and programs mainly developed for geological engineering and rock mechanics purposes have been applied to the study of slope stability on the flanks of volcanic edifices. These approaches provide relevant information

on factors that intervene in the instability processes and fault characteristics (Seisdedos et al., 2012).

In this work, the geomechanical characterization of five rock masses located on the southern flank of the Chiles Volcano was carried out; these values are complemented with results from other geomechanical studies developed in the area (on the east and north flanks of the volcano) from which different parameters of the rock mass are estimated.

2. GEOLOGICAL SETTING

Chiles Volcano is an active composite volcano in a resting state of the Cordillera Occidental, one of the three branches of the northernmost Andes (Colombian-Ecuadorian border). The volcanic arc results from the oblique subduction of the Nazca plate under the South American plate; specifically, Chiles Volcano is part of the southern volcanic segment of Colombia (an extension of northern Ecuadorian volcanism) that includes several volcanic complexes with active centers: Galeras, Azufral, Cumbal and, Chiles-Cerro Negro (Figure 1A; Monsalve-Bustamante, 2020); the southernmost of which is formed by Chiles Volcano and its neighbor, Cerro Negro de Mayasquer (Figures 1B and 1C).
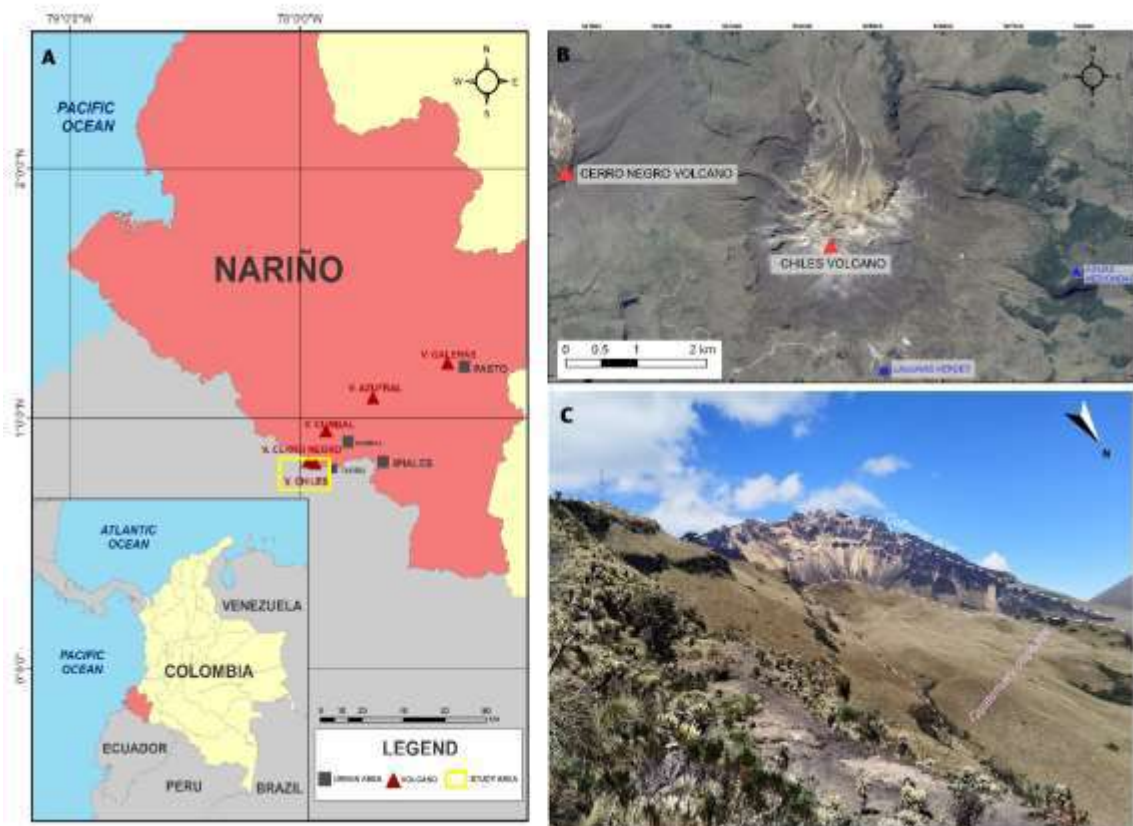
Figure 1. Location of Chiles Volcano. (A) Maps of Colombia and Nariño, showing the location of the volcanoes of the Southern Volcanic Segment of Colombia. (B) Google Earth satellite image showing Chiles and Cerro Negro volcanoes. (C) Panoramic photograph of Chiles Volcano collapse zone.

The current edifice of Chiles Volcano is formed by three lava outpouring episodes with units that preserve surface flow structures such as ogives (Figure 2). The first episode is characterized by the presence of pyroxene andesites and olivine andesites with a porphyritic texture. In erosive contact, the lavas of the second episode have a dacitic composition and exhibit a well-preserved flow structure. The third and final episode has a more basic composition, characterized by the presence of pyroxene and olivine andesites (Perdomo et al., 1986). Moreover, the hydrothermal alteration of these rocks is attributed to the action of high-temperature circulating fluids, as exemplified by the alterations (silicic and argillic) observed in the lavas (Perdomo et al., 1986; Velásquez and Parra, 2002; Usma et al., 2022).

According to radiometric data, Chiles Volcano was built during the Pleistocene; Ar/Ar radiometric dating indicates ages of 50.0 ± 5 ka (south flank), 53.0 ± 3 ka (southeast flank), and 57.2 ± 5 ka (north flank) (Telenchana et al., 2017). Geochemically, the lavas of Chiles Volcano are characterized by low contents of TiO$_2$ and elements of the potassium group; low concentration in LREE; low Ce/Yb ratio; and enrichment in HREE, with a high Ba/La ratio; these data are consistent with the partial melting of the oceanic crust or the mafic basement of the Cordillera Central and the Inter-Andean Graben, together with related fractional crystallization processes (Droux and Delaloye, 1996).

The volcanic edifice is located at the intersection area of several faults distributed in two main trends: WNW-ESE direction (transversal system) and NNE-SSW direction (longitudinal system) (Bocanegra and Sánchez, 2017). Notably, the Chiles – Cerro Negro and Chiles – Cumbal faults intersect near the highest zone of the volcanic edifice (Figure 2), where an area of intense hydrothermal alteration is identified. Manifestations of hot springs are associated with the Chiles-Cerro Negro fault at the place known as Aguas Hediondas (Perdomo et al., 1986); and the complex of three small lagoons called Lagunas Verdes, and the recently discovered hot springs of El Artezón are related with an unnamed fault (Figure 2; Bocanegra and Sánchez, 2017).
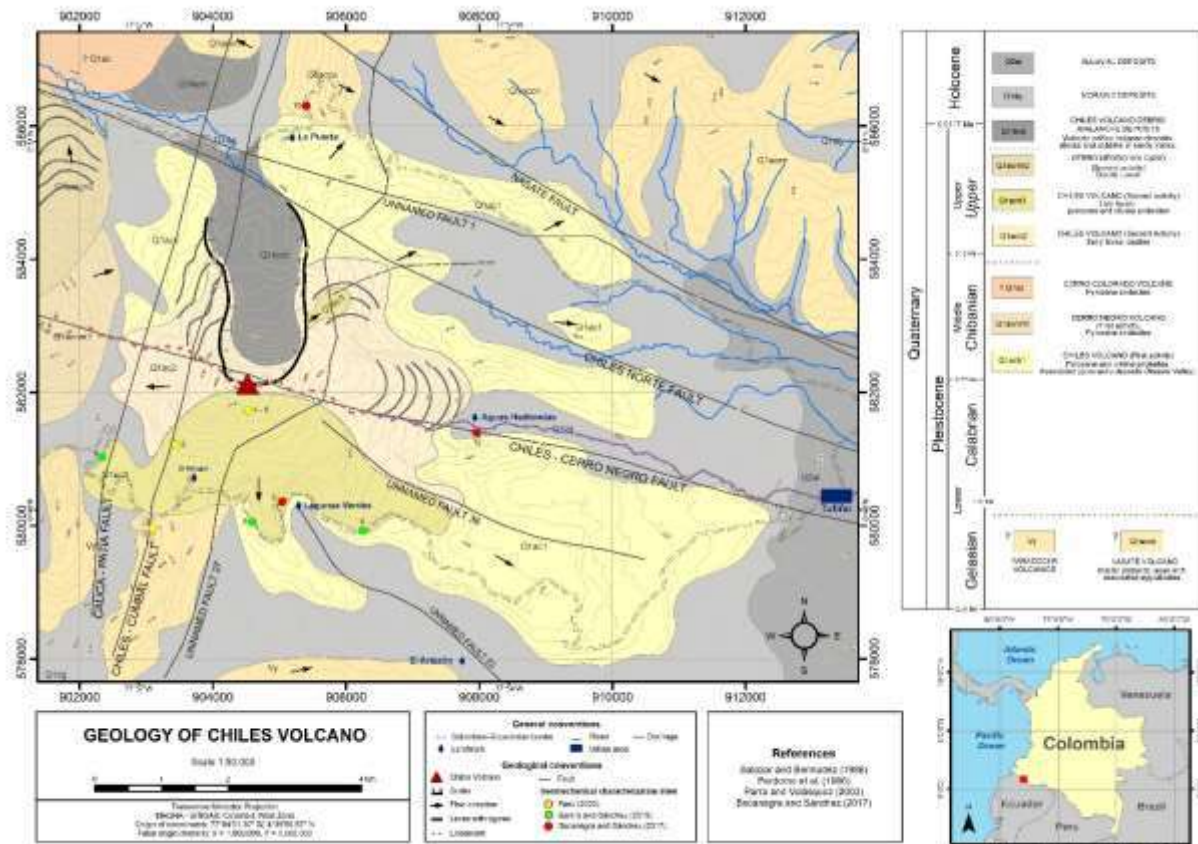

Figure 2. Chiles Volcano geological map. The numbers next to the geomechanical characterization sites are the points in Table 2. Coordinate system: MAGNA-SIRGAS/ Colombia West Zone. The map was made based on the geological cartography of Salazar and Bermúdez (1986); Perdomo et al. (1986); Parra and Velásquez (2003); and Bocanegra and Sánchez (2017).

Concerning the VDA deposits product of the lateral collapse on the northern flank of the volcano, it is estimated that only around 30% is preserved due to glacial and fluvial erosion in the area. The deposit is composed of angular blocks chaotically dispersed in a matrix of undescribed grain size, constituted by andesite fragments from the volcanic edifice (Velásquez and Parra, 2002).

3. MATERIALS AND METHODS

### 3.1 Delimitation and characterization of the Chiles Volcano collapse scar

The collapse scar of the northern flank of Chiles Volcano was delimited by integrating information from two main sources: the Convergence Index (CI; Figure 3A) calculated from an ALOS PALSAR Digital Elevation Model (DEM) of 12.5 m pixel size, and two superimposed polarimetric radar images taken by NASA's Uninhabited Aerial Vehicle Synthetic Aperture Radar (UAVSAR) of 1.8 m pixel size (Figure 3B).

Convergence Index (CI) is a morphological value that allows locating the divergent (crests) and convergent (valleys) features from the information of a DEM. Starting from a 3×3 neighborhood (analysis window) moving for each cell i, θ_i is the angle in degrees between the direction of the slope of the cell i (also known as aspect) and the direction of the vector joining the center of the cell i and the center of the window (Thommeret et al., 2010). This morphological parameter comprises values between 100 and -100 (equation 1; Jasiewicz, 2022), where positive values represent divergent zones and negative values represent convergent zones. In the case of null values, these are related to areas without curvature, such as flat slopes (Thommeret et al., 2010).

$$[1] \quad \text{CI} = \left[\left(\frac{1}{8} \sum_{i=1}^{8} \theta_i \right) - 90 \right] \frac{10}{9}$$

The digital terrain analysis program used in this study to calculate the CI was the System for Automated Geoscientific Analysis (SAGA; https://saga-gis.sourceforge.io/en/index.html), a tool that includes various geoscientific algorithms for the DEM analysis, facilitating the calculation of relevant parameters (Olaya and Conrad, 2009).

Complementary terrain parameters such as the aspect and the slope were used as supporting information for the visualization and delimitation of the scar. Other inputs to analyze the relief were photographs of the volcanic edifice provided by SGC and photos obtained in previous field campaigns carried out in the zone.
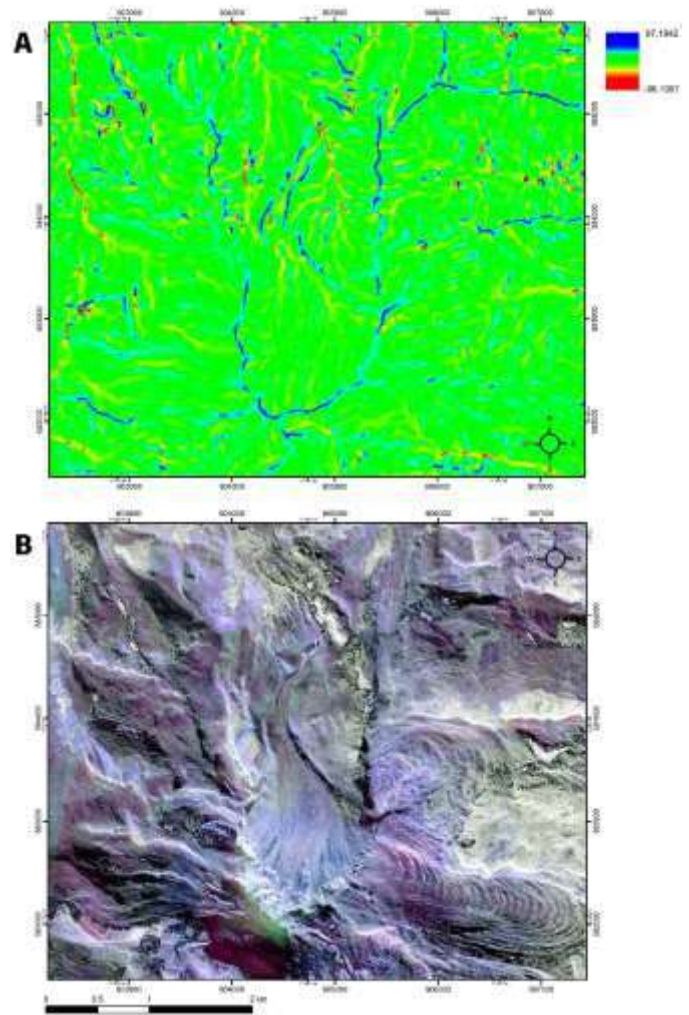
Figure 3. Convergence Index calculated for the area of interest. Values closer to 100 (blue tones) outline ridges, while values closer to -100 (red and yellow colors) highlight deep gullies. (B) UAVSAR mission L-band polarimetric SAR image of the area of interest with |HH-VV|, |HV|, and |HH+VV| as RGB channels. Modified from National Aeronautics and Space Administration (NASA) (2015).

Additionally, this information was analyzed in parallel with two superimposed UAVSAR images (flight line ID: EcuVol_11901 and EcuVol_29902), acquired on 17th March 2017 within the framework of NASA's airborne investigation focused on volcano deformation study (NASA, 2014). The radar operates in L-band at a central frequency of 1217.5 MHz to 1297.5 MHz, with a bandwidth of 80 MHz (range resolution of 1.8 m) and a swath width greater than 16 km. More information is available on the UAVSAR website (http://uavsar.jpl.nasa.gov/).

Radar images were visualized using QGIS Desktop 3.24.0 software through a Pauli color-coded file; this last one is based on linear combinations of the Synthetic Aperture Radar (SAR) polarimetric channels (HH, HV, VH, and VV). For this case, the polarimetric channels |HH-VV|, |HV| and |HH+VV| are assigned

to the RGB channels for displaying the image, respectively (Lee and Pottier, 2009).

Considering the elements of tone, texture, pattern, and form described by Mekel (1975) for the analysis and the interpretation of radar images applied to geology, the outline, and delimitation of the scar morphological expression was carried out.

The collapse scar was characterized following the methodology of Bernard et al. (2021), which divides it into three morphological elements: the wall, the limit with the greatest inclination of the scar (this is differentiated between the headwall, the one in front of the aperture, and the sidewall, which is parallel to the main direction of the slide); secondly, the floor, a relatively flat area; and finally, the aperture, the region between the lowest points of the sidewalls (Bernard et al., 2021). The quantitative description of the rupture zone was carried out by applying the parameters listed in Table 1.

Two superimposed irregular networks of triangles (TIN) were processed to calculate the Volume Scar (V_S) using Civil 3D 2023 Metric Volume Control Center tools (https://latinoamerica.autodesk.com/). The first input is the base surface, which was generated from the contour lines of 5 m interval extracted from the DEM of the rupture area. The second TIN, called comparison surface (TIN surface under which the volume is calculated), was generated from the intersection points of the collapse scar trace with the contour lines. The volume between these two TIN surfaces (base surface and comparison surface) is the data reported in this study.

3.2 Geomechanical characterization of the volcanic rocks

3.2.1 Outcrop characterization

The rock masses of Chiles Volcano were characterized in areas where lava flows crop out. These data, compared and integrated with geomechanical data obtained in previous works (Bocanegra and Sánchez, 2017; García and Sánchez, 2019) are presented in Table 2. Due to the difficulty of access imposed by the relief, weather conditions, and community restrictions, the fieldwork was carried out in accessible representative areas of the southern flank of the volcano (Figure 2). At sites where rock masses showed good preservation, the Rock Mass Rating (RMR) was applied. The geomechanical parameters considered in calculating the RMR were: the uniaxial compressive strength of intact rock, the degree of fracturing, the spacing and conditions of discontinuities, and the groundwater conditions (Bieniawski, 1989; See Supplementary material, Annex 1).

Table1. Quantitative parameters applied to characterize the volcanic landslide scar of the Chiles Volcano. *Parameters are subject to considerable variability if the pre- and post-avalanche topographies are poorly known. Source: Bernard et al. (2021), p. 58.

Acronym	Descriptive parameter	Description
L_S	Scar length	Distance from the headwall to the middle of the aperture
W_S	Scar width	Maximum distance between the sidewalls, orthogonal to the length
W_{SA}	Scar aperture width	Distance between the sidewalls at the aperture
H_S	Scar height	Height between the top of the headwall and the aperture
$\propto_S$	Scar aperture angle	Angle between the lines drawn from the headwall to the sidewalls extremity
β_S	Scar slope	Slope between the top of the headwall and the aperture $$\beta_S = arctan\ (H_S/L_S)$$
γ_S	Scar azimuth	Azimuth of L_S
A_S	Scar area	Surface of the scar in map view
D_{S^*}	Scar depth	Maximum depth of the scar between the pre- and post-landslide topography
V_{S^*}	Scar volume	Volume difference before and after the landslide
T_{S^*}	Scar thickness	Average thickness $$T_S = V_S/A_S$$
AR_S	Scar aspect ratio	Ratio between the average thickness and the radius of a circle of equal area $$AR_S = T_S/\sqrt{\left(\frac{A_S}{\pi}\right)}$$
EF_S	Elongation factor	Ratio between the scar length and width $$EF_S = L_S/W_S$$
CF_S	Closure factor	Ratio between the scar aperture width and the scar width $$CF_S = W_{SA}/W_S$$

For rock masses with poor rock quality, the RMR value is difficult to determine (Hoek and Brown, 1997; Jerram and Petford, 2011) thus the Geological Resistance Index (GSI) chart was applied to have a better estimation (Singh and Goel, 2011)

The joint condition factor (J_C) was calculated to obtain a more detailed description of the infill material of joints and discontinuities in the outcrops where the GSI was applied. This value depends on three parameters estimated in the field (equation 2): roughness (J_S), weathering (J_W), and the joint alteration factor (J_A) (Cai et al., 2004).

$$[2] \quad J_C = \frac{J_S J_W}{J_A}$$

3.2.2 Estimation of the mechanical properties of the rock mass through the Hoek-Brown and the Mohr-Coulomb criteria.

To calculate the strength properties of the rock mass (cohesion c', and friction angle Φ'), the Hoek-Brown and the Mohr-Coulomb criteria were applied using the RocData software (www.rockscience.com). The generalized Hoek–Brown criterion (Hoek et al., 2002) is expressed as:

$$[3] \quad \sigma'_1 = \sigma'_3 + \sigma_{ci}\left(m_b \frac{\sigma'_3}{\sigma_{ci}} + s\right)^a$$

Where σ'_1 and σ'_3 are the major and minor effective stresses at the time of the failure, respectively; σ_{ci} is the uniaxial compressive stress of the intact rock; s and a are constants assigned to the rock mass; and m_b is the Hoek-Brown material constant for the rock mass. This last value depends on the constant m_i for the intact rock block, which varies according to its petrographic and textural characteristics (Eberhardt, 2012).

m_b, s, and a are calculated through the following expressions:

$$[4] \quad m_b = m_i \, exp\left(\frac{GSI-100}{28 - 14D}\right)$$

$$[5] \quad s = exp\left(\frac{GSI-100}{9 - 3D}\right)$$

$$[6] \quad a = 0.5 + \frac{1}{6}\left(e^{-\frac{GSI}{15}} - e^{-\frac{20}{3}}\right)$$

As can be seen, the input parameters are the Geological Strength Index (GSI), the material constant m_i, and the disturbance factor D. The GSI is calculated for each case; in the outcrops where the RMR was estimated, this parameter was calculated by the empirical correlation established between these two criteria (Hoek and Brown, 1997). For all cases $m_i = 19$, the value designated for andesites (Hoek and Brown, 1997); in the case of D, for site 1 in table 2 the value $D = 0.7$ was considered because the rock mass showed mechanical removal processes, and for the other outcrops which were free of any type of intervention the $D = 0$ value was assigned (Hoek et al., 2002).

Table 2. Stations characterized geomechanically in the present and previous works. *Bocanegra and Sánchez (2017) originally named this station Aguas Hediondas (AH in this case).

Point	Site ID	Source	Geographical coordinates (°)		Method applied	Volcanic edifice flank
			Latitude	Longitude		
1	LVPM – 1		0.797429249	-77.94807937	GSI	S
2	LVPM – 2		0.808850762	-77.94494672		S
3	LVPM – 3	This study	0.801456881	-77.93078794	RMR	S
4	LVPM – 4A		0.813536943	-77.93520113		S
5	LVPM – 4B		0.813536943	-77.93520113	GSI	S
6	8		0.797181997	-77.91970200		SSE
7	10	García and Sánchez (2019)	0.800108379	-77.09308621		S
8	12		0.798372530	-77.93461406		S
9	18		0.807166689	-77.95487256	RMR	SW
10	LCBR – 12		0.854854595	-77.92734983		N
11	LCBR – 14	Bocanegra and Sánchez (2017)	0.801086171	-77.93059922		S
12	LCBR – AH*		0.810468901	-77.90433466		SE

From the Hoek-Brown parameters, equivalent values of the Mohr-Coulomb parameters (friction angle ϕ' and cohesion c') were calculated using RocData (Hoek et al., 2002). In this quantitative conversion, an average linear approximation to the non-linear envelope of the Hoek-Brown criterion is used for a range of minor principal stress values defined by $\sigma_t < \sigma_3 < \sigma'_{3\,max}$ (Hoek et al., 2002; Eberhardt, 2012). $\sigma'_{3\,max}$ is the upper limit of the confining stress over which the relationship of the Mohr-Coulomb and Hoek-Brown criteria is considered, and it is determined for each evaluated point (Hoek et al., 2002).

In the present study, $\sigma'_{3\,max}$ is calculated from formula 7, based on the slope height H, the global compressive stress of the rock mass σ'_{cm} (Hoek et al., 2002), and the unit weight γ. This last parameter for all rock masses, except for point 1 (see Table 2) was taken as $\gamma = 24\ kN/m^3$ (for massive lava flows), and for altered lava flows, $\gamma = 17\ kN/m^3$ (Seisdedos et al., 2012). Additionally, to calculate the equivalent Mohr-Coulomb strength parameters, a value of $\sigma_{ci} = 152\ MPa$ was considered, which corresponds to the uniaxial compressive stress of the intact rock established for andesites (RockMass, 2011).

$$[7] \quad \frac{\sigma'_{3\,max}}{\sigma'_{cm}} = 0.72 \left(\frac{\sigma'_{cm}}{\gamma H}\right)^{-0.91}$$

3.2.3 Triaxial compression test

Two cores were extracted from a sample collected from a coherent massive lavas outcrop located near the volcano scar, a few tens of meters from the highest and steepest point of the volcanic edifice, which makes this place one of the key sites to evaluate the resistance of the most recent lavas of the volcano (Point 4, Figure 2.

Additionally, the ideal sample conditions were met at the site, namely: (1) irregular rock fragment, an approximately 20 cm cubed sample; (2) rock with good competence; (3) low degree of weathering, and (4) that the planes of the joints that favor the extraction of the sample do not present any filling material adhered to the rock wall. These conditions lead to better results during drilling and extraction of the core on which the triaxial compression test is carried out. Photographs of the prepared and tested specimens are shown in Figure 4.

Macroscopically, the lava sample displays a porphyritic texture characterized by 50% to 60% of subhedral plagioclase crystals scattered within a dark gray or reddish aphanitic matrix. Some areas of the sample exhibit a fluid-like texture. Approximately 5% of pyroxene crystals are also visible, with their alteration potentially contributing to the reddish color of the sample (Figure 4).
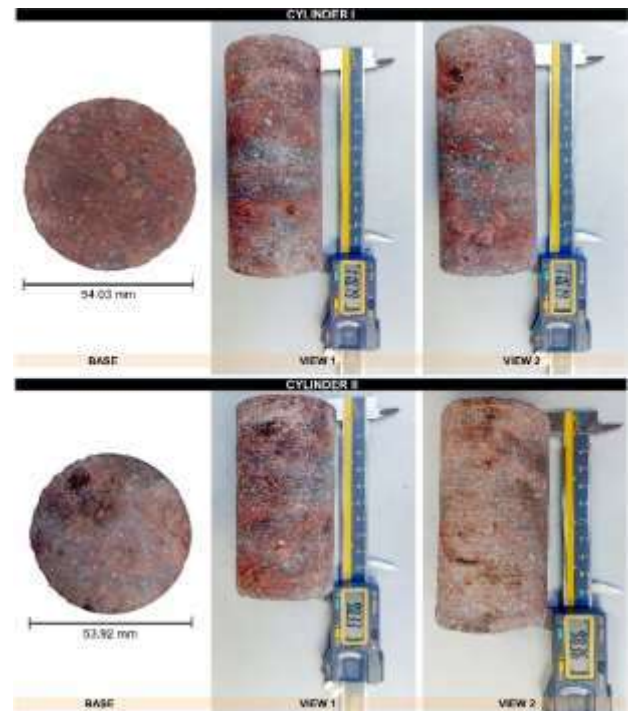

Figure 4. Photographs of the two andesite sample cores tested from Chiles Volcano, with their respective dimensions.

Through petrographic analysis the sample was classified as an andesite Le Maitre et al. (2002) with a hypocrystalline texture. It contains plagioclase, clinopyroxene, orthopyroxene, rutile, and sericite (due to the alteration of plagioclase). The rock has a flow-banded texture, vesicles, and corrosion bays in the pyroxenes; plagioclases are highly zoned, exhibit sieve texture, and some have polysynthetic twinning.

The CONTROLS Stress path triaxial and uniaxial automatic test system, administrated by the Rock Engineering Laboratory (Universidad Nacional de Colombia-Sede Medellín), was used to carry out the test. The applied method was the multiple failure test, also called the multi-step load triaxial compression test (ML-TCT; ISRM, 1983). This method allows the failure envelope and the strength parameters to be determined from a single sample in a series of stages, rather than using more than one rock cylinder as other conventional triaxial tests do (Taheri and Tani, 2009).

4. RESULTS

4.1 Chiles Volcano collapse scar

The Chiles Volcano scar in map view is U-shaped, with an approximately circular headwall and parallel sidewalls (Figure 5A). The scar has a length of approximately 3.0 km and its height is 0.8 km (Figures 5B and 5C). All geometric parameters determined for the scar are presented in Table 3.

The results of the cross-sectional analysis (Figure 6) show that the morphology of the northern flank of the volcano exhibits a smoother concave surface than the morphology of the southern flank.

The cross-sections perpendicular to L_S (profiles 2, 3, 4, 5 and 6; Figure 6) exhibits the steeply inclined sidewalls, and the floor with a generally flat slope. According to this, the scar is classified as deep-seated (Siebert and Roverato, 2021).

4.2 Geomechanical properties

The field observations indicate that the lava rock masses can be grouped into three main structural types: highly weathered brecciated lavas (Figure 7A), massive lava with columnar jointing (primary thermal contraction-induced joints) (Figures 7B and 7C), and lavas exhibiting a high degree of fracturing forming angular blocks, faceted, and not disintegrated (Figure 7D).

The results obtained from the geomechanical characterization carried out in the field are shown in Tables 4 and 5, respectively. The R5 grade (Hoek and Brown, 1997) was assigned for the uniaxial compressive strength of intact rock; this category includes a range of 100 to 120 MPa. The RMR' and GSI' values were calculated from empirical correlation (Hoek and Brown, 1997), considering a value of 15 for groundwater conditions (parameter 5 of the RMR, see supplementary material). The empirical correlation does not apply for the LVPM – 1 site (Table 5) because the equation is valid for GSI values ≥18 (Singh and Goel, 2011).

Table 3. Geometric parameters of the Chiles Volcano scar. *Parameters are subject to considerable variability if the pre- and post-avalanche topographies are poorly known. Bernard et al. (2021).

Acronym	Descriptive parameter	Value
L_S	Scar length	3.0 km
W_S	Scar width	1.6 km
W_{SA}	Scar aperture width	1.7 km
H_S	Scar height	0.8 km
$\propto_S$	Scar aperture angle	31°
β_S	Scar slope	14.9°
A_S	Scar area	4.0 km²
γ_S	Scar azimuth	0°
V_{S^*}	Scar volume	0.5 km³
T_{S^*}	Scar thickness	0.1 km
AR_S	Scar aspect ratio	0.1
EF_S	Elongation factor	1.85
CF_S	Closure factor	1.07
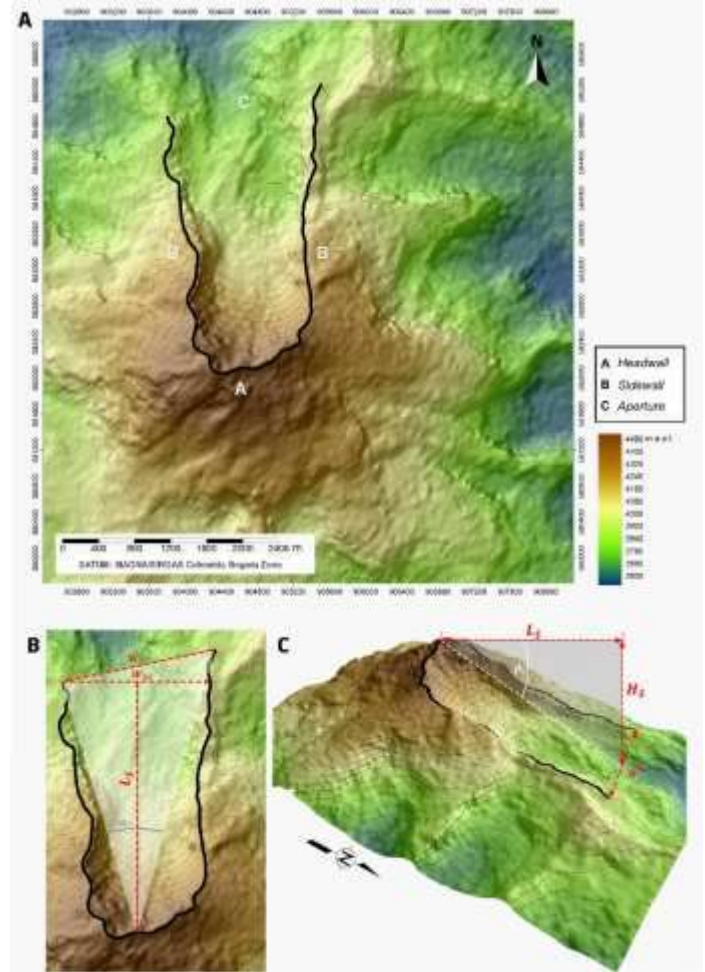
Figure 5. Morphological expression of the Chiles Volcano's collapse scar. (A) Morphological elements of the scar. Plan view (B) and perspective view (C) of the collapse sector, showing some geometric parameters (see Table 1 for its definition).

The strength parameters obtained from the triaxial compression test by the multiple failure method are presented in Table 6. The empirical correlation does not apply for the LVPM – 1 site because the equation is valid for GSI values ≥ 18 (Singh and Goel, 2011).

5. DISCUSSION

There are some limitations associated with the morphological characterization of the scars produced by the lateral collapse of a volcanic edifice. The delimitation, description, and geometric analysis of the Chiles Volcano scar are based on the current morphological expression of the volcanic edifice. As the collapse happened at least 20 ka (Velásquez and Parra, 2002), the volcanic edifice has been exposed to other processes that could have influenced the resulting original morphology.

From a geological perspective, this timeframe is remarkably brief for typical erosion processes occurring within equatorial climates to create a landform of such immense scale, remarkably preserved and clearly delineated on the volcanic edifice.

This is why in this study the data from the original scar are extrapolated to current conditions. It is suggested that future field control should be carried out in the aperture zone, since the continuations of the scar limbs are not clear near the end. Additionally, future additional calculations on the erosion rates of the area are recommended to broaden the perspective on the influence of other erosional processes on the evolution of this landform.

Chiles Volcano collapse scar was classified as deep-seated with a U-shape. This classification represents the first approach to the analysis of the instability factors and the possible mechanisms that triggered the collapse (Bernard et al., 2021; Roverato et al., 2021). Deep-seated scars have been associated with processes that affect the volcanic edifice at great depths, such as cryptodome intrusions or highly altered volcanoes cores (Bernard et al., 2021). The U-shape is associated with faults that originate or propagate from the basement (Bernard et al., 2021). The

triggering mechanisms related to these morphological characteristics are not directly associated with magmatic activity.

Geological evolution of the Chiles Volcano does not evidence cryptodomes intrusions (Perdomo et al., 1986; Cortés and Calvache, 1996; Dorux and Delaloye, 1996; Velásquez and Parra, 2002; Pinilla et al., 2008; Telenchana et al., 2017), but this volcano is characterized by the presence of many hydrothermal vents on its flanks (Perdomo et al., 1986; Cortés and Calvache, 1996; Velásquez and Parra, 2002; Usma et al., 2022; Taussi et al., 2023). Although the characteristics of the volcano's hydrothermal system change over time (circulating fluid rate, temperature, infiltration of meteoric water, etc.) (Roverato et al., 2021), since the transverse profile parallel to the direction of the collapse (figure 6) indicates a deep-seated scar and considering the large number of thermal springs in the area, hydrothermal activity might have promoted the instability of the volcanic edifice before the collapse of the northern flank. The above highlights the significant importance of morphological analysis in the collapse area, especially given the limited documentation of the VDA deposits in this instance. (Velásquez and Parra, 2002).
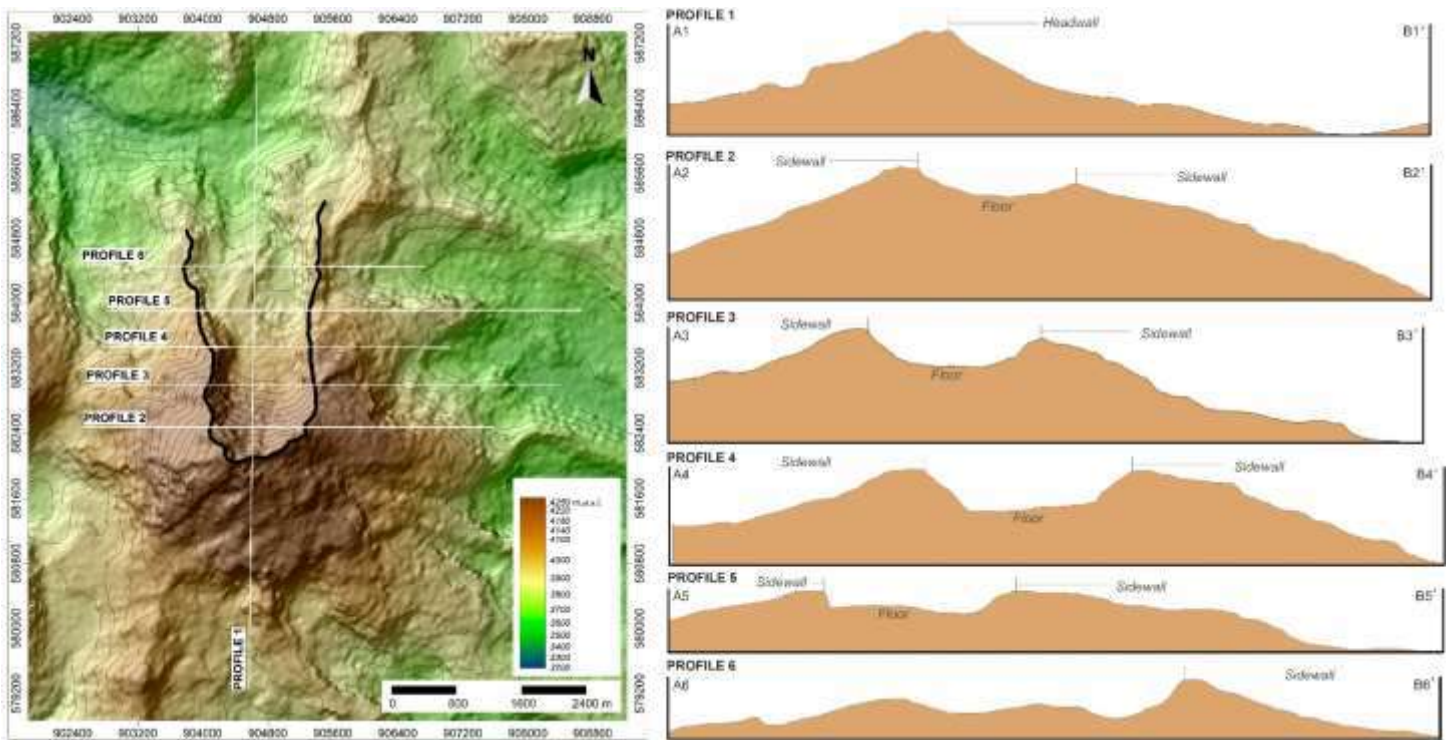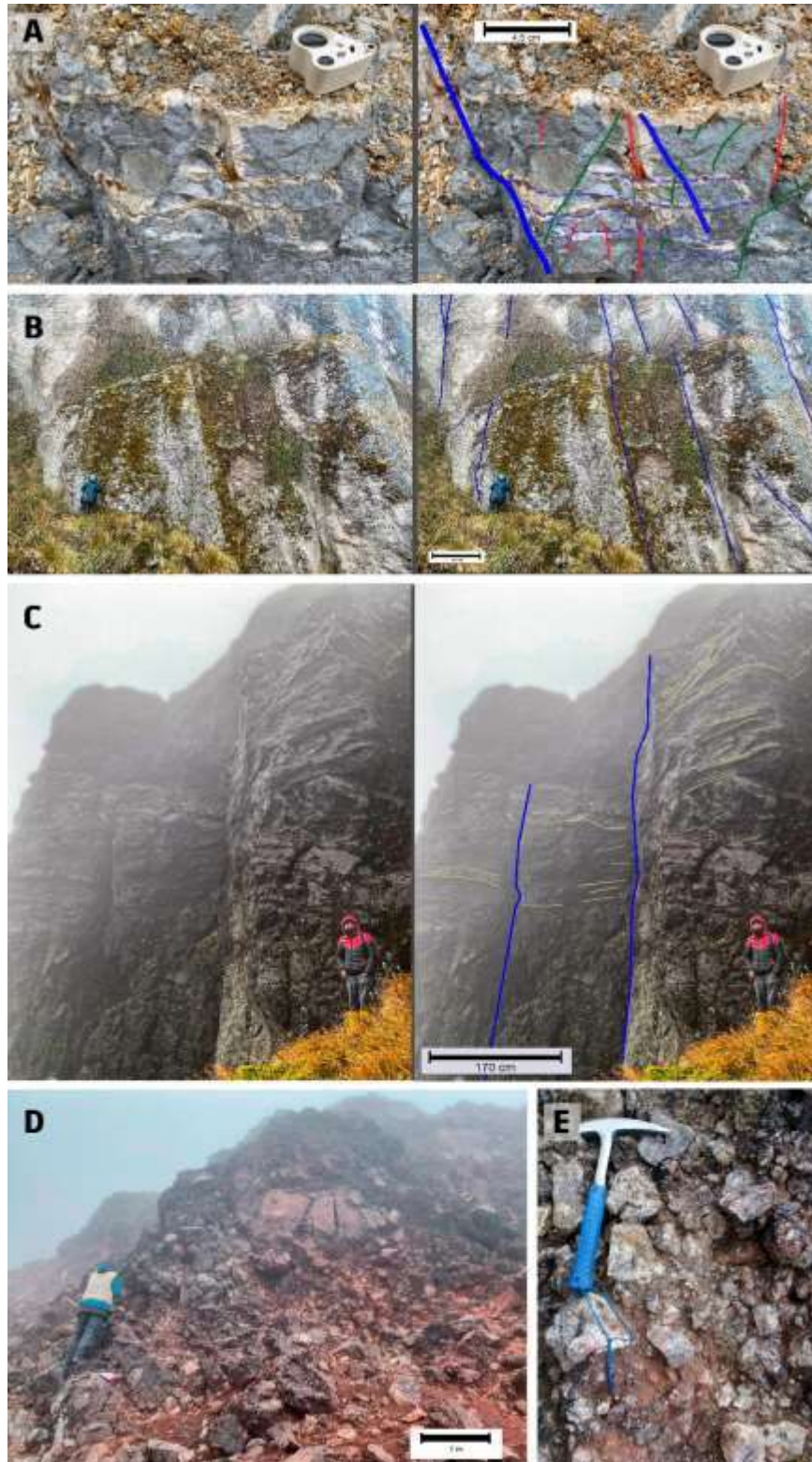

Figure 6. Cross-sections parallel and perpendicular to the scar length (L_S), indicating spatial variations of the morphological elements of the scar.

Figure 7. Representative sections of the lavas that were characterized geomechanically. (A) Highly weathered lava flow breccia; on the right photo families of joints are delineated with different colors; (B), (C) Characteristic columnar jointing of the Chiles Volcano lavas; the blue lines in the photographs on the right indicate the major joints of thermal origin; (D) Blocky lavas with a chaotic arrangement of angular blocks, varying in shape from slightly smoother to curved, some reaching up to a meter in diameter; and (E), more detailed view of (D). These lavas exhibit extensive fracturing, where a primary set of joints is not clearly identifiable. GSI was applied to these outcrops.

Table 4. Compilation of Rock Mass Rating (RMR) parameters determined for Chiles Volcano lava flows. New data from the sites characterized geomechanically in the present work plus data from previous works (see table 2 for references and conventions). The estimated Geological Strength Index (GSI) values are also shown. See the supplementary material for the RMR parameters.

Point	Station ID	Predominant lithology and fabric	1	2 %RQD	2 Value	3	4B A	4B B	4B C	4B D	4B E	5	RMR	GSI'
2	LVPM - 2	Lava flow with columnar jointing with centimetric corded surfaces	12	92	20	10	2	0	5	6	5	10	70	65
3	LVPM - 3	Massive lava flow with columnar jointing	12	100	20	5	2	0	6	6	3	10	64	59
4	LVPM - 4A	Considerably weathered reddish lava flow with columnar jointing	12	89	17	10	5	0	5	4	5	10	68	63
6	8	Lava flow with columnar jointing and secondary multiple jointing	12	92	20	10			20			4	66	61
7	10	Lava flow with vertical columnar jointing	12	94	20	10			25			10	77	72
8	12	Lava flow with columnar jointing	12	95	20	10			0			10	52	47
9	18	Lava flow with columnar jointing predominant at the base	12	98	20	15			20			10	77	72
10	LCBR - 12	Lava flow with columnar jointing, crossed by a spring	12	94	20	-			-			-	77	72
11	LCBR - 14	Brecciated lava flow with hydrothermal alteration	12	44	8	-			-			-	70	65
12	LCBR - AH*	Lava flow with columnar jointing close to hot spring	12	78	17	-			-			-	73	68

Table 5. Compilation of Rock Mass Rating (RMR) parameters determined for Chiles Volcano lava flows. New data from the sites characterized geomechanically in the present work plus data from previous works (see table 2 for references and conventions). The estimated Geological Strength Index (GSI) values are also shown. See the supplementary material for the RMR parameters.

Point	Station ID	Predominant lithology	GSI	J_S	J_W	J_A	J_C	RMR'
1	LVPM – 1	Brecciated lava flow with very high weathering	15	1.5	1	1	1.5	N/A
5	LVPM - 4B	Blocky lavas	47	2	2	2	2	52

Table 6. Results of the triaxial compression test Cylinder I, sample LVPM – 4A.

		Peak	Residual	Unit
Mohr-Coulomb Parameters	Cohesion	4.21	1.52	MPa
	Friction Angle	51.95	52.4	°
	Compressive strength	24.42	---	MPa
	Rock Failure Mechanism	Shear fracture of intact rock		

VDA deposits sedimentological description indicates that pumice is not present in the debris avalanche deposit generated by the collapse (Velásquez and Parra, 2002). Moreover, given that the volcano was predominantly composed of lava flows and no evidence of eruptive activity was observed after the collapse, it is plausible that the northern flank of the Chiles Volcano collapsed without the influence of erupting activity. However, a specific relationship between the scar morphology and its origin has not yet been established (Bernard et al., 2021).

Analyzing Chiles Volcano U-shaped scar within the tectonic configuration of the area, the azimuth of the collapse ($\gamma_S = 0°$) and the lateral walls orientation of the scar tend to be parallel to the direction of the longitudinal faults (SW-NE direction), and perpendicular to the transverse fault system (SE-NW direction). Additionally, the trend of these descriptive parameters is approximately perpendicular to the direction of the main tectonic stress, calculated in N 97.2°± 19.3° (Sierra, 2015).

Different studies worldwide show that the movement of basement faults affects the stability of the overlying volcanic edifice, and these can even propagate into it (Roverato et al., 2021). Many morphological and structural characteristics, including collapse directions, are configured according to regional stress fields. In numerous volcanoes, the failure scar openings normal to the fracture planes parallel to the main stress field have been associated with collapse events (Siebert, 1984). As an example of this, there are 28 examples of breaches cones in the Central Andes (Francis and Wells, 1988) and 30 Japanese volcanoes (Siebert, 1984).

Nevertheless, in many other cases collapse directions do not show a specific relationship with the regional stress field (Roverato et al., 2021), the collapse direction is approximately at right angles to the tectonic elements parallel to the direction of the regional stress field: Chiles-Cerro Negro Fault and the transverse fault system described by Bocanegra and Sánchez (2017). This suggests that the tectonic configuration of the Chiles Volcano area is a factor that significantly influences the stability of the volcanic edifice, and that seismic activity was a possible triggering factor for collapse.

Regarding the volume of the scar ($V_S = 0.5\ km^3$) and its area ($A_S = 4.0\ km^2$), these values are within the range of values that have been reported in other collapse cases (Siebert and Roverato, 2021); however, it is suggested to apply other methods of calculation for future comparisons, since the calculations were made considering the current conditions of the scar, but not carrying out the reconstruction of the volcano edifice.

Finally, the reliability of in situ geomechanical studies is often limited by geological complexity and logistical difficulties.

Applying empirical rock mechanics criteria (in this case, Hoek-Brown, and Mohr-Coulomb criteria) to estimate geomechanical parameters that cannot be obtained in any other way implies uncertainties and constitutes a limitation (Seisdedos et al., 2012). However, these results can be useful for other researchers who study the instability of the flanks of andesite volcanoes (the composition of most Colombian volcanoes).

6. CONCLUSSIONS

The characterization and analysis of the morphological expressions resulting from the lateral collapse of a volcanic edifice represent a first approach to the possible triggering mechanisms. Scars may represent the only element available to study these processes in volcanic areas with a poor sedimentological record of the debris avalanche deposits.

In this work, the morphological expression product of the collapse of the northern flank of the Chiles Volcano was delimited, identifying the three morphological elements of the scar (headwall, sidewall, and aperture) and reporting new data regarding its geometry. The deep-seated scar and its U-shape, together with the sedimentological evidence reported in the literature for the debris avalanche deposit, suggest that the collapse was possibly unrelated to eruptive activity.

The geomechanical properties of the outcropping rocks on the flanks of the Chiles Volcano were obtained from the geomechanical characterization in the field, the application of empirical mechanical rock criteria, and triaxial laboratory tests. This information was also complemented with data from the literature to estimate the strength parameters of Chiles Volcano andesites.

Finally, this study will further support future geomechanical models of the volcanic edifice, which will also allow for a more profound understanding of the factors that destabilize the flanks and trigger lateral collapses.

CONFLICT OF INTEREST

The authors declare that they have no known competing financial interests or personal relationships that could have appeared to influence the work reported in this paper.

SUPPLEMENTARY MATERIAL

Annex 1. Table S1. Parameters of the RMR System introduced by Bieniawski (1989) including the descriptive terms presented by Singh and Goel (2011). Modified from Bieniawski (1989).

See: https://doi.org/10.32685/0120-425/bol.geol.51.1.2024.714

REFERENCES

Bernard, B., Takarada, S., Andrade, D., and Dufresne, A. (2021). Terminology and strategy to describe large volcanic landslides and debris avalanches. In M. Roverato, A. Dufresne, and J. Procter (Ed.), Volcanic Debris Avalanches: from Collapse to Hazard, Advances in Volcanology. Springer. https://doi.org/10.1007/978-3-030-57411-6_3

Bieniawski, Z. (1989). Engineering Rock Mass Classifications: A Complete Manual for Engineers and Geologists in Mining, Civil, and Petroleum Engineering. John Wiley & Sons, Inc., United States.

Bocanegra, L., and Sánchez, J. (2017). Mapa de Fallas de Los Volcanes Chiles-Cerro Negro (Nariño) a Partir de Minería de Datos y Confirmación de Campo. Boletín de Geología, 39(3), 71–86. https://doi.org/10.18273/revbol.v39n3-2017005.

Cai, M., Kaiser, H., Uno, Y., Tasaka, and Minami, M. (2004). Estimation of Rock Mass Deformation Modulus and Strength of Jointed Hard Rock Masses Using the GSI System. International Journal of Rock Mechanics and Mining Sciences, 41(1), 3–19. https://doi.org/10.1016/S1365-1609(03)00025-X

Cortés, G., and Calvache, M. (1996). Investigación sobre la evolución y composición de los volcanes de Colombia: Galeras y volcanes del sur (explanatory memory). INGEOMINAS.

Droux, A., and Delaloye, M. (1996). Petrography and Geochemistry of Plio-Quaternary Calc-Alkaline volcanoes of Southwestern Colombia. Journal of South American Earth Sciences, 9(1-2), 27–41. https://doi.org/10.1016/0895-9811(96)00025-9

Eberhardt, E. (2012). The Hoek – Brown Failure Criterion. Rock Mechanics and Rock Engineering, 45, 981–88. https://doi.org/10.1007/s00603-012-0276-4

Francis, PW., and Wells, GL. (1988). Landsat Thematic Mapper observations of debris avalanche deposits in the Central Andes. Bulletin of Volcanology, 50, 258-278. https://doi.org/10.1007/BF01047488

García, Y., and Sánchez, J. (2019). Contribuciones geológicas al modelo conceptual geotérmico en la región de los volcanes Chiles – Cerro Negro (Colombia-Ecuador). Boletín de Geología, 41(1), 151–71. https://doi.org/10.18273/revbol.v41n1-2019008

Hoek, H., and Brown, E. (1997). Practical estimates of rock mass strength. International Journal of Mechanics and Mining Sciences, 34, 1165-1168. https://doi.org/10.1016/S1365-1609(97)80069-X

Hoek, H., Carranza-Torres, C., and Corkum, B. (2002). Hoek-Brown Failure Criterion – 2002 Edition. Proc. NARMS-TAC Conference, Toronto. https://www.researchgate.net/publication/282250802_Hoek-Brown_failure_criterion_-_2002_Edition

Instituto de Hidrología, Meteorología y Estudios Ambientales (IDEAM). (n.d.-b). Normales Climatológicas Estándar_Periodo 1991-2020 (Technical report). Retrieved from http://www.ideam.gov.co/web/tiempo-y-clima/clima

Instituto de Hidrología, Meteorología y Estudios Ambientales (IDEAM). (n.d.-a). Clasificaciones climáticas Colombia (Technical report). Retrieved from http://www.ideam.gov.co/documents/21021/21789/climas+%5BModo+de+compatibilidad%5D.pdf/d8c85704-a07a-4290-ba65-f2042ce99ff9

International Society for Rock Mechanics and Rock Engineering (ISRM). (1983). Suggested methods for determining the strength of rock materials in triaxial compression: Revised version. International Journal of Rock Mechanics and Mining Sciences & Geomechanics Abstracts, 20(6), 285–290. https://doi.org/10.1016/0148-9062(83)90598-3

Jasiewicz, J. (2022, July 10). r.convergence - Calculate convergence index. GRASS GIS 7.8.8dev. https://grass.osgeo.org/grass82/manuals/addons/r.convergence.html#:~:text=Convergence%20index%20is%20mean%20(or,10%2F9%20%3D%20-100.

Jerram, D., and Petford, N. (2011). The Field Description of Igneous Rocks. John Wiley & Sons, Ltd., Chichester.

Joya, L. (2013). Estudio de la relación entre la orientación de las fallas y las estructuras de las avalanchas de escombros en volcanes (bachelor tesis). Universidad Nacional de Colombia, Bogotá, Colombia.

Karátson, D., Németh, K., Székely, B., Ruszkiczay-Rüdiger, Zs., and Pécskay, Z. (2006). Incision of a river curvature due to exhumed Miocene volcanic landforms: Danube Bend, Hungary. International Journal of Earth Sciences (GR Geologische Rundschau), 95, 929–944. https://doi.org/10.1007/s00531-006-0075-9

Lee, J., and Pottier, E. (2009). Polarimetric Radar Imaging from Basics to Applications. CRC Press, Boca Raton.

Le Maitre, R. W., Streckeisen, A., Zanettin, B., Le Bas, M. J., Bonin, B. and Bateman, P. (eds) (2002). Igneous Rocks: A Classification and Glossary of Terms: Recommendations of the International Union of Geological Sciences Subcommission on the Systematics of Igneous Rocks. Cambridge University Press. https://doi.org/10.1017/CBO9780511535581

Mead, S., Procter, J., Bebbington, M., and Rodriguez-Gomez, C. (2022). Probabilistic Volcanic Hazard Assessment for National Park Infrastructure Proximal to Taranaki Volcano (New Zealand). Frontiers Earth Sciences, 10, 832531. https://doi.org/10.3389/feart.2022.832531

Mekel, J. (1975). Geological interpretation of radar images. Journal of the Indian Society of Photo-Interpretation, 3, 1–19. https://doi.org/10.1007/BF03007908

Monsalve-Bustamante, M. (2020). The volcanic front in Colombia: Segmentation and recent and historical activity. In J. Gómez, and A.O. Pinilla–Pachon (Ed.), The Geology of Colombia. https://www2.sgc.gov.co/LibroGeologiaColombia/tgc/sgcpubesp38201903.pdf

Moreno, S., Sánchez, J., and Murcia, H. (2021). Evidences of an unknown debris avalanche event (<0.58 Ma), in the active azufral

volcano (Nariño, Colombia). Journal of South American Earth Sciences, 107, 103138. https://doi.org/10.1016/j.jsames.2020.103138

National Aeronautics and Space Administration (NASA). (2010). Dataset: © JAXA/METI ALOS PALSAR ALPSRP275270010 2010. Accessed through https://asf.alaska.edu/ June 2022.

National Aeronautics and Space Administration (NASA). (2014). NASA Airborne Research Focuses on Andean Volcanoes. Available at: https://www.nasa.gov/jpl/uavsar/volcanoes-20140527/ (Accessed: July 2022).

National Aeronautics and Space Administration (NASA). (2015). Dataset: UAVSAR, NASA 2015. Retrieved from https://asf.alaska.edu/ June 2022.Olaya, V., and Conrad, O. (2009). Chapter 12: Geomorphometry in SAGA. Developments in Soil Science, 33, 293 – 308. https://doi.org/10.1016/S0166-2481(08)00012-3

Parra, E., and Velásquez, M. (2003). Geología de la Plancha 447 Ipiales – 447Bis Tallambí, sheets 447 – 447Bis. Scale 1:100 000. INGEOMINAS.

Perdomo, G., Ardila, R., and Meneses, L. (1986). Estudio geológico para prospección de azufre en el área de Cumbal – Chiles – Mayasquer (Nariño) (bachelor tesis). Universidad Nacional de Colombia, Bogotá, Colombia.

Pinilla, A., Ríos, P., Rodríguez, B., Sánchez, J., Pulgarín, B., Borrero, C., and Roa, H. (2008). El Neógeno Volcánico En El Altiplano Nariñense, Suroccidente Colombiano. Geología Colombiana, 33, 69-78. https://revistas.unal.edu.co/index.php/geocol/article/view/32049

Procter, J.N., Cronin, S.J., Platz, T., Patra, A., Dalbey, K., Sheridan, M., and Neall, Vince. (2010). Mapping block-and-ash flow hazards based on Titan 2D simulations: a case study from Mt. Taranaki, NZ. In: J. Clague, F. Comiti, T. Glade, J. Goff., and H. Gupta. (Ed.) Natural Hazards. Springer. https://doi.org/10.1007/s11069-009-9440-x

Procter, J.N., Zernack, A.V., Cronin, S.J. (2021). Computer Simulation of a Volcanic Debris Avalanche from Mt. Taranaki, New Zealand. In: M. Roverato, A. Dufresne, J. Procter. (Ed.) Volcanic Debris Avalanches. Advances in Volcanology. Springer, Cham. https://doi.org/10.1007/978-3-030-57411-6_11

Roverato, M., Di Traglia., D., Procter, J., Paguican, E., and Dufresne, A. (2021). Factors Contributing to Volcano Lateral Collapse. In M. Roverato, A. Dufresne, and J. Procter (Ed.), Volcanic Debris Avalanches: from Collapse to Hazard, Advances in Volcanology. Springer. https://doi.org/10.1007/978-3-030-57411-6_5

RockMass. (2011). Uniaxial compressive strength (σ_c) and deformation modulus of rocks. Available at: https://rockmass.net/files/strength_and_deform_values%20.pdf (Accessed: July 2022).

Seghedi, I., Szakács, A., Mirea, V., Pécskay, Z., Luffi, P. (2023). Volcanic debris avalanche deposits and their significance in the architecture and evolution of the Miocene-Quaternary Călimani-Gurghiu-Harghita volcanic range (Eastern Transylvania, Romania). Journal of Volcanology and Geothermal Research, 443, 107932. https://doi.org/10.1016/j.jvolgeores.2023.107932

Salazar, E., and Bermúdez, R. (1986). Hoja Geológica Tulcán, escala 1:100000. Scale 1:100 000. Instituto de Investigación Geológico y Energético – IIGE.

Seisdedos, J., Ferrer, M., and González de Vallejo., L. (2012). Geological and geomechanical models of the pre-landslide volcanic edifice of Güímar and La Orotava mega-landslides (Tenerife). Journal of Volcanology and Geothermal Research, 239–240, 93-110. https://doi.org/10.1016/j.jvolgeores.2012.06.013

Servicio Geológico Colombiano (SGC). (2014). Mapa de Amenaza Volcánica del Volcán Chiles. Scale 1:50.000.

Servicio Geológico Colombiano (SGC). (2021). Generalidades Volcán Chiles. Available at: https://www2.sgc.gov.co/sgc/volcanes/Volcan-Chiles/Paginas/generalidades-volcan-chiles.aspx. (Accessed March 3, 2021).

Siebert, L. (1984). Large volcanic debris avalanches: characteristics of source areas, deposits, and associated eruptions. Journal of Volcanology and Geothermal Research, 22, 163-197. Elsevier Science Publishers B.V. https://doi.org/10.1016/0377-0273(84)90002-7

Siebert, L., and Roverato, M. (2021). A historical perspective on lateral collapse and debris avalanches. In M. Roverato, A. Dufresne, and J. Procter (Ed.), Volcanic Debris Avalanches: from Collapse to Hazard, Advances in Volcanology. Springer. https://doi.org/10.1007/978-3-030-57411-6_2

Sierra, E. (2015). Determinación del estado de esfuerzos tectónicos en la zona del Complejo Volcánico Chiles- Cerro Negro (bachelor tesis). Escuela Politécnica Nacional, Quito, Ecuador.

Singh, B., and Goel, R. (2011). Geological Strength Index. Engineering Rock Mass Classification, 319–334. https://doi.org/10.1016/B978-0-12-385878-8.00026-4

Taheri, A., and Tani, K. (2009). Developing a generalized multiple-step loading damage model to predict rock behaviour during multiple-step loading triaxial compression test. 17th International Conference on Soil Mechanics and Geotechnical Engineering (Volumes 1, 2, 3 and 4), Egypt. doi:10.3233/978-1-60750-031-5-429

Telenchana, E., Bernard, B., and Hidalgo, S. (2017). Modelo evolutivo del Volcán Chiles. VIII Jornadas en Ciencias de la Tierra, Quito.

Taussi, M., Tardani, D., and Tassi, F. (2023). A conceptual model for the Tufiño-Chiles-Cerro Negro (TCCN) geothermal system (Ecuador-Colombia): New insights into geothermal exploration from chemical and isotopic composition of hydrothermal fluids. Journal of Geochemical Exploration, 249, 107214. https://ui.adsabs.harvard.edu/link_gateway/2023JCExp.24907214T/doi:10.1016/j.gexplo.2023.107214

Thommeret, N., Bailly, J., and Puech, C. (2010). Extraction of thalweg networks from DTMs: application to badlands. Hydrology and Earth System Sciences, 14, 1527–1536. https://doi.org/10.5194/hess-14-1527-2010

Usma, D., Sánchez, J., and Bonilla, G. (2022). Caracterización de alteraciones para exploración geotérmica en el Volcán Chiles, frontera colombo-ecuatoriana. XV Semana Técnica de Geología, Ingeniería geológica y Geociencias, Barranquilla. https://www.researchgate.net/publication/363475731_Caracterizacion_de_alteraciones_para_exploracion_geotermica_en_el_Volcan_Chiles_frontera_colombo-ecuatoriana

Van Wyk de Vries, B., and Davies, T. (2015). Chapter 38 - Landslides, Debris Avalanches, and Volcanic Gravitational Deformation. In H.

Sigurdsson, B. Houghton, S. McNutt, H. Rymer, and J. Stix (Ed.), The Encyclopedia of Volcanoes. Elsevier. https://doi.org/10.1016/B978-0-12-385938-9.00038-9

Velásquez, M., and Parra, E. (2002). Geología de Las Planchas 447 - Ipiales y 447 BIS – Tallambí (explanatory memory). INGEOMINAS.